www.czasopisma.pan.pl PAN www.journals.pan.pl

ARCHIVES of FOUNDRY ENGINEERING

DE GRUYTER OPEN

ISSN (2299-2944)
Volume 17
Issue 1/2017

DOI: 10.1515/afe-2017-0027

Published quarterly as the organ of the Foundry Commission of the Polish Academy of Sciences

147 – 152

SiMo Ductile Iron Crystallization Process

M. Stawarz
Silesian University of Technology, Department of Foundry,
Towarowa 7, 44-100 Gliwice, Poland
Corresponding author. E-mail address: marcin.stawarz@polsl.pl

Received 29.06.2016; accepted in revised form 16.08.2016

Abstract

The article presents crystallization process of silicon molybdenum ductile cast iron (SiMo). The alloy with 5% silicon content and with variable amounts of Mo in a range of 0-1% was chosen for the research. The carbon content in the analysed alloys did not exceed 3,1%. The studies of crystallization process were based on thermal – derivative analysis (TDA). Chemical composition of all examined samples was analysed with the use of LECO spectrometer. Additionally, the carbon and the sulphur content was determined basing on carbon and sulphur LECO analyser. For metallographic examination, the scanning electron microscopy (SEM) with EDS analyser was used. Disclosed phases have been also tested with the use of X-ray diffraction. The results allowed the description of crystallization processes of silicon molybdenum ductile cast iron using thermal – derivative analysis (TDA). Conducted studies did not allow for the clear identification of all complex phases containing molybdenum, occurring at the grain boundaries. Therefore, the further stages of the research could include the use of a transmission electron microscope to specify the description of complex compounds present in the alloy.

Keywords: Crystallization process, Silicon cast iron, SiMo, TDA

1. Introduction

The article presents crystallization process of silicon molybdenum ductile cast iron (SiMo) basing on TDA analysis. In paper [1] an attempt to describe the crystallization process of SiMo cast iron designed for work in petrochemical conditions was made. However, the methodology of the research did not take into account the TDA analysis, which gives a broad spectrum of information about the analyzed alloys. While in the paper [2] thermal – derivative analysis was used, the tested alloy containing the addition of molybdenum cannot be classified as a cast iron from SiMo type because of the low Si content. The same applies to the results presented in [3], additionally, the research refers to the combined effect of Cr and Mo on the crystallization process. Accordingly, this paper presents analysis of three experimental melts with different Mo content and the description of the crystallization processes. It proposed a variable content of Mo in the range of 0-1% in increments of 0,5% Mo. Adoption of such research topic is associated with an extremely advantageous properties of described cast iron during the work in elevated temperatures. The most important advantages of cast iron containing from 4-6% silicon is low price, good oxidation resistance, dimensional stability, high resistance to high operating temperatures, thermal shock and temperature cycling resistance [4-6].

For most applications, the Mo content in the range of 0,5 to 1% provides the appropriate strength in elevated temperature and creep resistance. Higher additions of molybdenum are used, when it is necessary to maximize strength at higher temperature. High molybdenum addition, more than 1% causes the formation of interdendritic type Mo_2C carbides which are stable even after annealing and decrease the strength and ductility of the alloy in room temperature [7].

The content of molybdenum in SiMo cast iron defines the specific application of alloy:

- 0,0-0,5% for applications with large and fast cycling temperatures,

- 0,5-1,0% for applications with creep (long time in high temperature),
- 1,5-2,0% for applications that require a high strength in high temperature (creep resistance or very high temperature) [7].

The main applications of SiMo cast iron are: exhaust manifolds for combustion engines, gas turbine components, moulds for casting of zinc, titanium and brass alloys, stands, holders for heat treatment (cyclic temperature changes), the elements of furnaces for heat treatment etc.

2. Description of the work methodology

Presented paper attempts to describe crystallization process of low silicon alloy cast iron with variable molybdenum content. Experimental melts were conducted in the induction furnace with medium frequency and the capacity of 25kg. The charge consisted of steel scrap with low sulphur content. Other ingredients added during the melting was ferrosilicon (FeSi75), RANCO carburizer and FeMo65 rich alloy. The spheroidization process of cast iron was conducted in the bottom of the ladle, after covering the nodulizing agent by pieces of steel scrap. Magnesium rich alloy used in the studies was FeSiMg5RE. The TDA analysis was conducted using Crystaldigraph NT-2T [8] converter with the Electronite cup-shaped tester with shell mould that contained NiCr-Ni thermocouple (K-type). During melting the temperature of liquid metal in the furnace was controlled by immersion thermocouple (type S). Samples for chemical analysis were taken from the ladle after the spheroidization of cast iron. In the experimental melts the pre-degassing of liquid metal in the furnace used in production of silicon cast iron [9-11] was not carried out because of the relatively low Si content in analysed cast iron.

3. Research results

Table 1 shows the results of chemical composition analysis for the analysed experimental melts. Presented chemical compositions were defined based on the LECO spectrometer analysis. Additionally, the carbon and the sulphur contents were determined basing on carbon and sulphur LECO analyser. Results shown in the table 1 include corrected values for C and S.

Table 1.
Chemical composition of ductile cast iron

Alloy	Element content, % wt.						
No.	C	Si	Mo	P	Mn	S	Mg
1	3.02	5.03	0,01	0.021	0.368	0.009	0.032
2	2.94	5.14	0.37	0.020	0,453	0.005	0.029
3	3.04	4.94	1.09	0.022	0.421	0.005	0.031

In the next stage of the research the results from the thermal-derivative analysis have been elaborated. Figures 1-3 present graphs of temperature changes in time, supplemented by the value of the first derivative of temperature over time for better identification of characteristic points and areas of crystallizing phases in examined alloys.

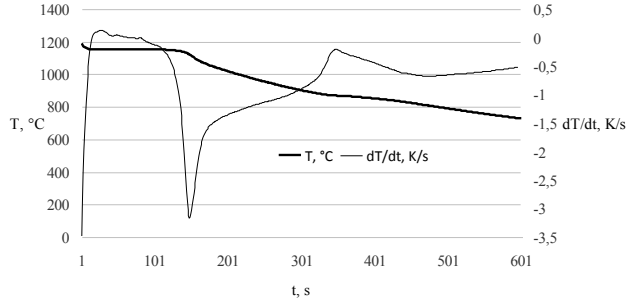

Fig. 1. TDA analysis for alloy without Mo content. Alloy No. 1

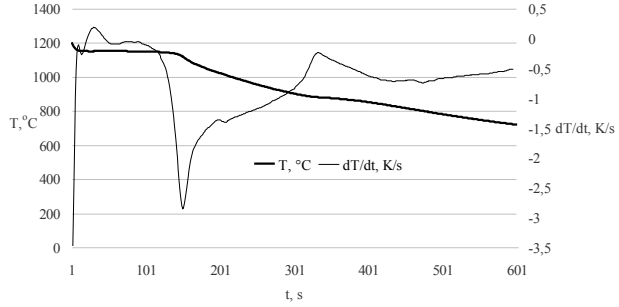

Fig. 2. TDA analysis for alloy with 0,37% Mo content. Alloy No. 2

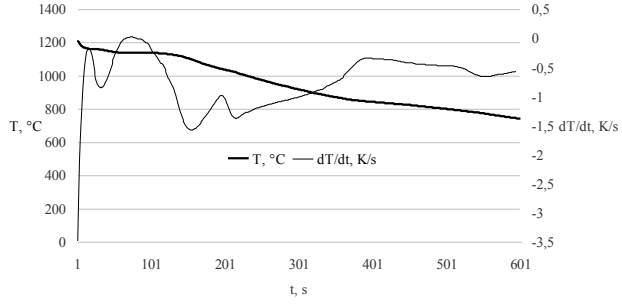

Fig. 3. TDA analysis for alloy with 1,09% Mo content. Alloy No. 3

Character of presented graphs from TDA analysis for alloy 1 and 2 is basically very similar. The 0,37% addition of Mo resulted in slight thermal effect shown in Figure 2 around 201s of registration measurement. The maximum value of thermal effect corresponds to 1015°C temperature. It is thought that this effect is due to the crystallisation of the secondary carbide phase rich in Mo.

Figure 3 shows analysed alloy containing 1,09% Mo. The aforementioned thermal effect is very clearly visible and as in the previous case, the maximum value was registered after 201s of measurement. The temperature value which corresponds to the maximum point of the effect in this case is 1031°C. With the

increase of Mo content the temperature range and the time of phase transformation γ+graphite+M_xC → α+γ+graphite+M_xC → α+graphite+M_xC in the range of 900°C-766°C temperature is also changing, which is very well visible in Figure 3.

In order to confirm the results obtained from TDA analysis the metallographic examination was performed using scanning electron microscopy with EDS analysis. Figures 4-6 present fractures of examined alloys.

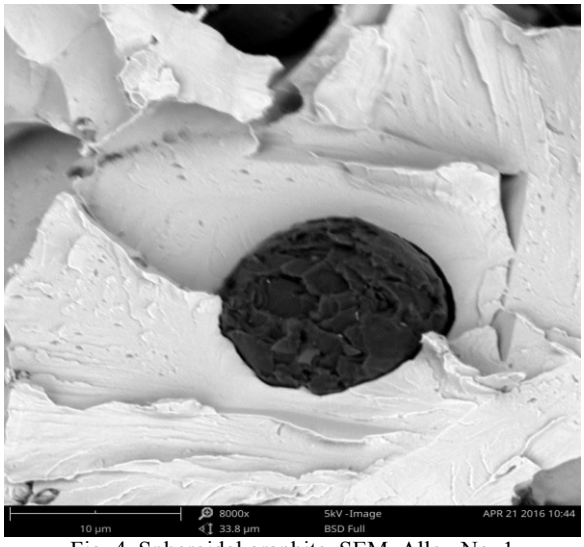

Fig. 4. Spheroidal graphite, SEM. Alloy No. 1

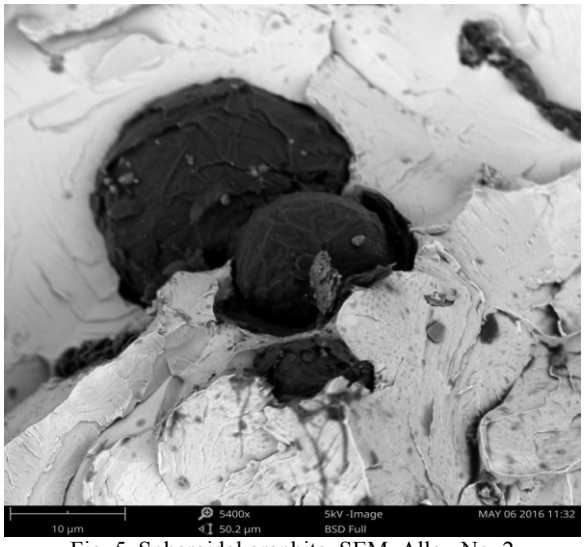

Fig. 5. Spheroidal graphite, SEM. Alloy No. 2

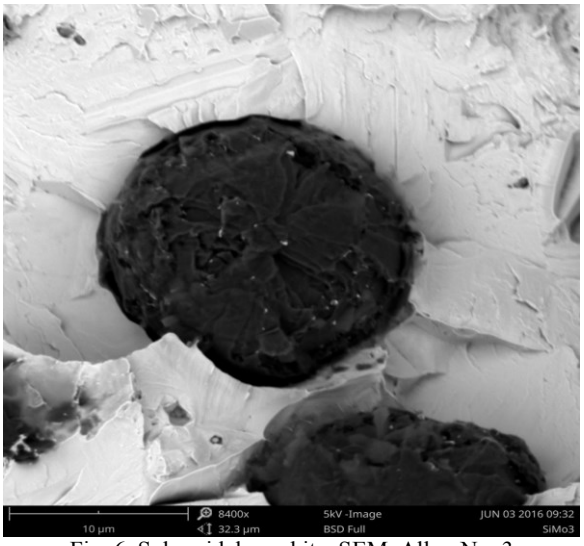

Fig. 6. Spheroidal graphite, SEM. Alloy No. 3

In all three cases the nodular graphite precipitations on analysed fractures were shown. The chemical composition (Table 1) shows the low residual magnesium content, which should be an obstacle to the crystallization of spheroidal graphite, however, the conducted chemical analysis due to the applied patterns, along with the method of analysis did not allow to identify the other elements favouring the spheroidization process (eg. Ce, La) which content in the nodulizing agent was less than 1%.

In the next stage of studies metallographic sections were analysed. The SEM and EDS (energy dispersive X-ray spectroscopy) analysis were performed. Figures 7-10 present obtained results.

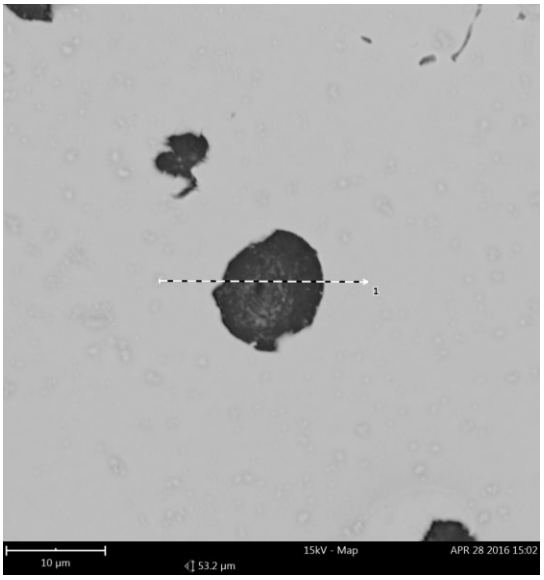

Fig. 7. SiMo alloy No. 1 without Mo addition

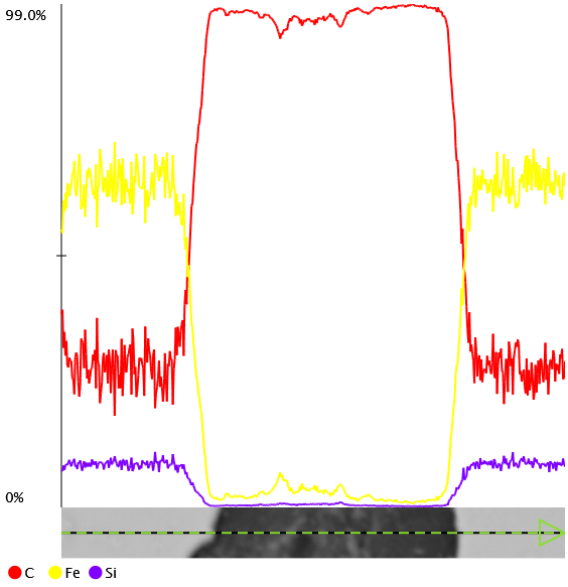

Fig. 8. SiMo alloy No. 1 without Mo addition. Linea scan of spheroidal graphite

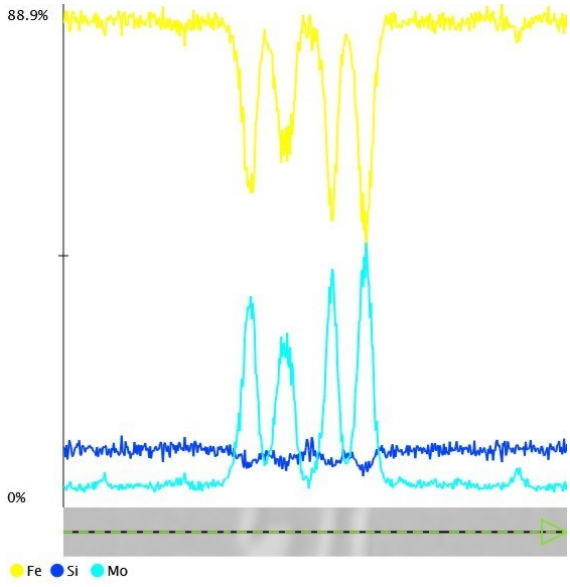

Fig.10. SiMo alloy No. 2 with 0,37% Mo addition. Linea scan of multi-phase

For alloy marked as No. 1 (with no added Mo) in analyzed microstructure the nodular graphite precipitations were found in the homogeneous ferritic matrix. Minor discolorations visible on Figure 7 are due to the limitations of used scanning electron microscope. Figure 8 show the linear analysis for the precipitation of nodular graphite. The analysis confirmed presence of graphite. Figures 9-10 present the results of metallographic analysis of the alloy designed as No. 2 containing 0.37% Mo. In the microstructure of the analysed alloy the compounds containing increased amount of Mo were founded on the grain boundaries of ferrite, as shown in Figure 10 as a linear scan.

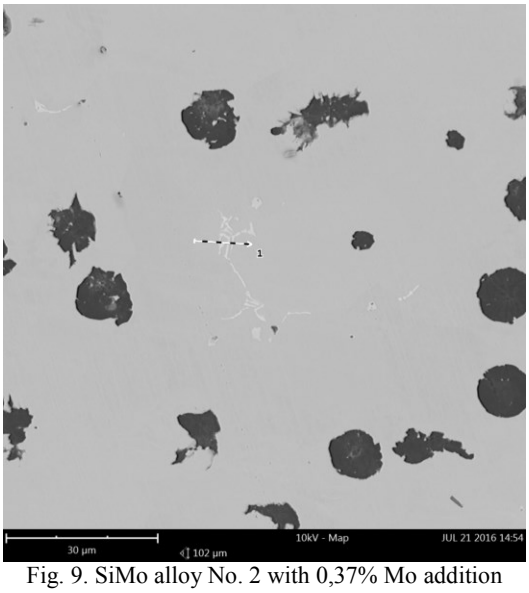

Fig. 9. SiMo alloy No. 2 with 0,37% Mo addition

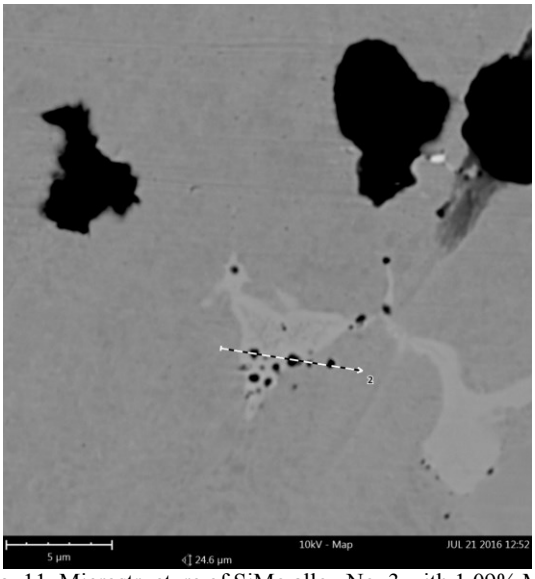

Fig. 11. Microstructure of SiMo alloy No. 3 with 1,09% Mo addition

Figure 11 presents complex compound in the form of bright precipitation with black spots. Also, the precipitations of degenerate nodular graphite are visible. For identification of the precipitation the line scan across the disclosed precipitation were executed. The method of analysis is shown with the arrow with the index 2 in Figure 11.

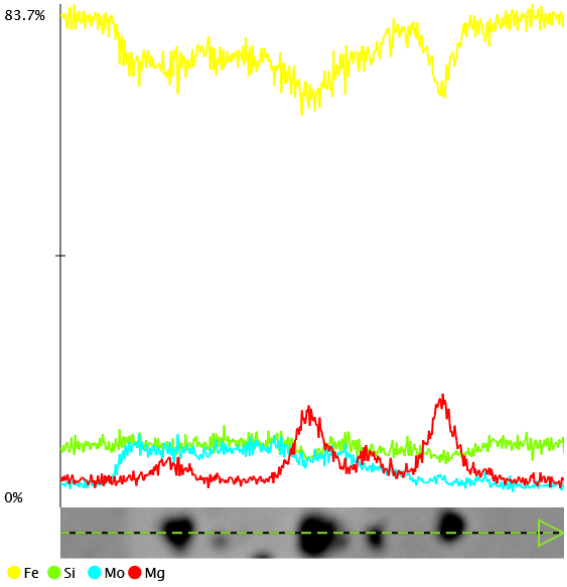

Fig. 12. SiMo alloy No. 3 with 1,09% Mo addition. Linea scan of multi-phase

From the results (Fig. 12), the following elements are present: Fe, Si, Mo, Mg. Additionally, Figure 13 presents the analysis with graph showing a linear Mg content in this precipitation. Dark areas on the analysed precipitation are much richer in this element (Mg).

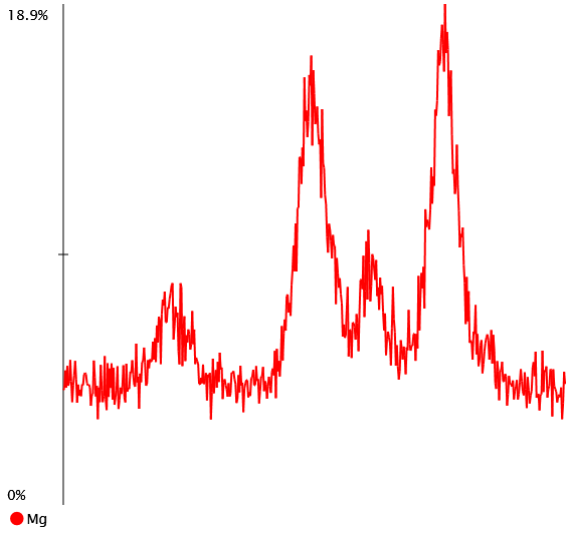

Fig. 13. SiMo alloy No. 3 with 1,09% Mo addition. Linea scan of magnese

The next step was the X-ray microanalysis. The results are presented in the form of a diffraction pattern in Figure 14.

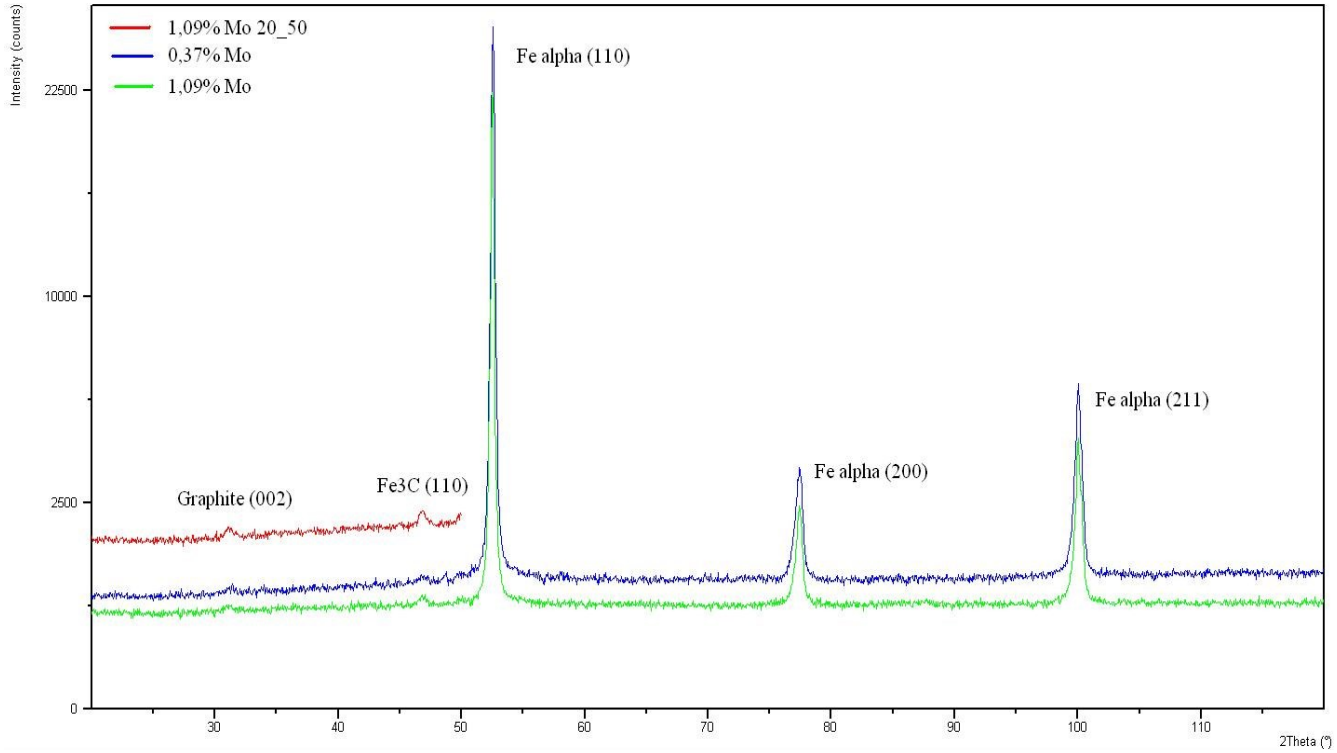

Fig. 14. Diffractions graph for analyzed alloys

Samples No. 2 and No. 3 were tested (Samples containing Mo, where on the grain boundaries the bright carbide phase appears). It was decided to not conduct the similar studies for alloy No. 1, because in this sample there are spheroidal graphite precipitations in the ferritic matrix.

As it is shown in Figure 14 there are ”strong” lines for Fe. Additionally, a measurement in a long time was performed in the range of angles visible before the line of Fe, which allowed to show diffraction lines for graphite and cementite in the sample containing 1,09% of Mo.

4. Conclusions

In presented studies the application of TDA analysis allowed to precisely determine the temperature scope of transition for the analysed alloys. With the increasing content of Mo the temperature range and time of phase transformation γ+graphite+$M_xC \rightarrow \alpha+\gamma$+graphite+$M_xC \rightarrow \alpha$+graphite+$M_xC$ in the temperature range of 900°C-766°C were changed, which is very clearly registered for the melt No. 3.

Also, compounds of Mo formed at the grain boundaries were found. Unfortunately, used research tool did not allow to confirm results from work [1], where a minor Fe_2MoC phase precipitations and smaller amounts two-phase aggregates of Fe_2MoC/M_6C were noticed. Also Mg segregation at the grain boundaries was observed, but conducted studies did not allow to identify the phases. Paper [1] describes results which shows that the Mg demonstrated the ability to segregate at the grain boundaries and formed $MgSiN_2$ compound, but the specific conditions, which was not in conducted studies may exclude the presence of such compounds.

The measurement in a long time in the range of angles visible before the line of Fe allowed to show diffraction lines for type (2H) graphite and Fe_3C in the sample containing 1,09% of Mo. The further stages of research may contain the use of a transmission electron microscope to specify the description of the present complex compounds.

References

[1] Magnusson Åberg L. & Hartung C. (2012). Solidification of simo Nodular cast iron for high temperature applications. *Trans Indian Inst Met.* 65(6), 633–636. DOI 10.1007/s12666-012-0216-8.

[2] Pietrowski, S. & Pisarek, B. (1997). Crystallization and structure chromium-molybdenum cast iron. *Solidification of Metals and Alloys.* 30, 191-202. (in Polish).

[3] Pietrowski, S. & Gumienny, G. (2006). Crystallization of ductile cast iron with Mo, Cr, Cu and Ni. *Archives of Foundry.* 6(22), 406-413. (in Polish).

[4] Delprete, C., Sesana, R. & Vercelli, A. (2010). Multiaxial damage assessment and life estimation: application to an automotive exhaust manifold. *Procedia Engineering.* 2, 725-734. DOI:10.1016/j.proeng.2010.03.078.

[5] Matteis, P. Scavino, G., Castello, A. & Firrao, D. (2014). High temperature fatigue properties of a Si-Mo ductile cast iron. *Procedia Materials Science.* 3, 2154- 2159. DOI: 10.1016/j.mspro.2014.06.349.

[6] Guzik, E. & Wierzchowski, D. (2012). Using cored wires injection 2PE-9 method in the production of ferritic Si-Mo ductile iron castings. *Archives of Foundry Engineering.* 12(4), 53-56.

[7] Stefanescu, D.M. (1998). *Casting.* Volume 15. (4th ed.). International ASM Handbook.

[8] Szajnar, J., Dulska, A., Wróbel, T. & Baron, C. (2015). Description of alloy layer formation on a cast steel substrate. *Archives of Metallurgy and Materials*. 60(3), 2367-2372. DOI: 10.1515/amm-2015-0386.

[9] Stawarz, M. (2013). Influence of technological parameters on the microstructure of the silicon cast iron, In Metal 2013: 22nd International Conference on Metallurgy and Materials. Ostrava. TANGER 2013, pp. 92-96.

[10] Stawarz, M., Gromczyk, M., Jezierski, J. & Janerka, K. (2015). Analysis of the high silicon cast iron crystallization process with TDA method. In Metal 2015: 24th International Conference on Metallurgy and Materials. Ostrava: TANGER 2015, pp. 42-47.

[11] Stawarz, M., Janerka, K., Jezierski, J. & Szajnar, J. (2014). Thermal effect of phase transformations in high silicon cast iron. In Metal 2014: 23rd International Conference on Metallurgy and Materials. Ostrava: TANGER 2014, pp.123-128.